Processing and Application of Ceramics 18 [4] (2024) 375–385
https://doi.org/10.2298/PAC2404375V

Structure and magnetic properties of epitaxial Sr-$LaMnO_3$ thin films obtained by polymer assisted deposition

Jelena Vukmirović[1], Danica Piper[1], Pavla Šenjug[2], Damir Pajić[2], Bojan Miljević[2], Marija Milanović[1], Sara Joksović[1,3], Mirjana Novaković[4], Vladimir V. Srdić[1,5,*]

[1]*Department of Materials Engineering, Faculty of Technology Novi Sad, University of Novi Sad, Bul. Cara Lazara 1, 21000 Novi Sad, Serbia*
[2]*Department of Physics, Faculty of Sciences, University of Zagreb, Horvatovac 102a, 10000 Zagreb, Croatia*
[3]*Biosense Institute, University of Novi Sad, Zorana Đinđića 2, 21000 Novi Sad, Serbia*
[4]*Department of Atomic Physics, Vinča Institute of Nuclear Sciences - National Institute of the Republic of Serbia, University of Belgrade, M. Petrovića Alasa 12-14, 11351 Vinča, Belgrade, Serbia*
[5]*Serbian Academy of Sciences and Arts, Kneza Mihajla 35, 11000 Belgrade, Serbia*

Received 18 September 2024; Received in revised form 9 November 2024; Accepted 29 November 2024

Abstract

Epitaxial $La_{1-x}Sr_xMnO_3$ (LSMO, where x = 0, 0.1, 0.3 and 0.5) films on single crystal $SrTiO_3$ (001) substrate were obtained by water-based chemical solution deposition method, so-called polymer assisted deposition (PAD). The as-prepared films (heated at 750 °C for 1 h) have thicknesses of ~30 nm, high uniformity, clear and well-defined interface and crack-free surfaces. In addition, they are characterized by the formation of an imperfect crystal structure with some disoriented areas, small amount of non-stoichiometric phase and defects created just to support the epitaxial film growth. During multiple annealing at different temperatures up to 900 °C epitaxial nature was preserved in all LSMO films. The structure rearrangement through elimination of defects and formation of unit cell closer to the corresponding bulk stoichiometric phase were observed. The magnetic properties of the LSMO thin films were measured using SQUID magnetometer in the temperature range of 5–400 K with the field applied parallel (in-plane) and perpendicular (out-of-plane) to the film surface. The angle dependence of the magnetic moment in the LSMO thin films at the room temperature was also measured by a vibrating sample magnetometer.

Keywords: *Sr-doped $LaMnO_3$, epitaxial thin films, structure, electric and ferromagnetic properties*

I. Introduction

Thin films play an important role in the development of microelectronics and offer a huge contribution to the miniaturization, improving the performance of electronic devices and lowering the energy consumption. Various methods have been used to fabricate thin films, but for those that are widely used in microelectronics, vapour phase deposition techniques have been dominant for a long time. Those techniques are usually associated with high costs, so chemical solution deposition methods have been adapted recently for such applications. There are different variants of chemical solution deposition, but sol-gel is the most attractive and the most frequently used with various modifications [1–3].

Transition metal oxides with perovskite structures exhibit a variety of unusual properties, including ferromagnetism, ferroelectricity or multiferroic behaviour, making them excellent candidates for various integrated magnetic and electronic devices [4–6]. In particular, manganite based thin films are recognized as good candidate for low-power-consumption spintronic devices [7–9]. $LaMnO_3$ (LMO) has a cubic perovskite structure that is distorted at room temperature (RT) into an orthorhombic structure due to a strong Jahn-Teller interaction. It is well-known that bulk LMO is an insulator and A-type antiferromagnetic [10,11], but the presence of defects (such as cation or oxygen vacancies) might have

*Corresponding author: +381 21 450 3665
e-mail: *srdicvv@uns.ac.rs*

strong influence on LMO properties. For example, La-deficient samples tend to be ferromagnetic and metallic [12]. These modifications of the bulk properties could also be induced by stress due to the mismatch between the film and the substrate, as it can cause stoichiometry changes and lattice distortion. Because of such critical stoichiometry issues, the growth of LMO thin films is not a trivial achievement [10]. The mismatch can force formation of the misfit dislocations at the film/substrate interface, but also other structural changes, such as conversion of manganese ions from Mn^{3+} to Mn^{4+}, formation of non-stoichiometric phases, etc. [13–15]. Thus, strain engineering strategy might be very useful in designing an appropriate structure for miniature spintronic devices. In this respect doping can also be very helpful.

LMO structure could be easily doped with different cations, such as: Sr^{2+}, Ca^{2+}, Ba^{2+} etc. forming an interesting class of compounds where the interplay between metal-insulator and ferromagnetic-paramagnetic transitions results in a variety of fascinating properties such as colossal magnetoresistance [16–18]. Thus, combination of doping and strain engineering strategies offers enormous possibilities. In particular, $La_{1-x}Sr_xMnO_3$ ($0.17 \leq x \leq 0.5$) thin films show strong ferromagnetic properties, large magnetoresistance and high conductivity, which make them suitable for spintronic devices [6,19]. The ferromagnetic behaviour is associated with the double exchange effect between Mn^{3+} and Mn^{4+} ions via oxygen $2p$ orbitals, so the Mn^{3+}/Mn^{4+} ratio plays an important role in the magnetic and conductive properties of the material [20,21].

In the previous work, we studied LMO thin films prepared by modified sol-gel method, so-called polymer assisted deposition (PAD) technique and deposited on MgO and $SrTiO_3$ single crystal substrates [14]. A highly oriented growth of LMO films was observed despite the epitaxial strain caused by a certain lattice mismatch. In order to accommodate this strain, different defects as well as a non-stoichiometric phase were formed, introducing Mn^{4+} ions and thus influencing the Jahn-Teller distortions. However, the additional thermal treatment was proven to be an effective way to tune the lattice distortion of manganite films, changing the symmetry of the lattice towards the stoichiometric phase.

In this work, we present the results related to the structure and magnetic properties of the $La_{1-x}Sr_xMnO_3$ thin films on $SrTiO_3$ (001) substrate. The obtained results confirmed the formation of the epitaxial LSMO thin films on top of the $SrTiO_3$ substrate. The data also indicated the change of the pseudocubic perovskite unit cell towards orthorhombic and/or rhombohedral symmetry with Sr addition, while magnetic measurements confirmed the ferromagnetic behaviour of the films with higher Sr content at RT.

II. Experimental

The $La_{1-x}Sr_xMnO_3$ (LSMO, where x = 0, 0.1, 0.3 and 0.5) epitaxial ultra-thin films were prepared by the water-based chemical solution deposition method, so-called polymer assisted deposition (PAD) technique following the procedure reported earlier [14]. Lanthanum-manganite based solutions (0.1 M) were obtained by dissolving La^{3+}, Mn^{2+} and optionally Sr^{2+} nitrates ($La(NO_3)_3 \cdot 6H_2O$, ≥99.0%, Fluka; $Mn(NO_3)_2 \cdot 4H_2O$, ≥99.0%, Fisher Chemical and $Sr(NO_3)_2$, ≥99.0%, Sigma Aldrich) in water with ethylene-diamine-tetraacetic acid (EDTA) and polyethyleneimine (PEI $M_w \sim 25000$ by LC, $M_n \sim 10000$ by GPC). EDTA at a concentration of 7 wt.% and PEI (mass ratio 1:1 to EDTA) were used as chelating agents to improve stability, viscosity and surface tension of the solutions by complexation with metal ions. The prepared solutions were spin-coated onto single crystal $SrTiO_3$ (001) substrates (previously cleaned by ethanol) to prepare uniform layers for post-treatment (Fig. 1). The deposited layers were thermally treated at 750 °C in air to remove solvents/organics and form a crystalline structure (the as-prepared oxide films). In the next step, the as-prepared films were annealed in air at different temperatures up to 900 °C to follow the structural changes of the films as a function of thermal treatment.

The epitaxial nature and phase composition of the $La_{1-x}Sr_xMnO_3$ thin films were examined by X-ray diffraction on Rigaku MiniFlex 600 diffractometer using Cu-K_α radiation in the range 20–60°, and in-plane measurements were performed by using Rigaku Smart Lab diffractometer. For detailed microstructural analysis, cross-sectional lamellae of the thin films were prepared by focus ion beam (FIB) in a FEI Scios 2 Dual Beam system and observed using conventional and high-resolution transmission electron microscopy (TEM/HRTEM) on FEI Talos F200X transmission electron microscope.

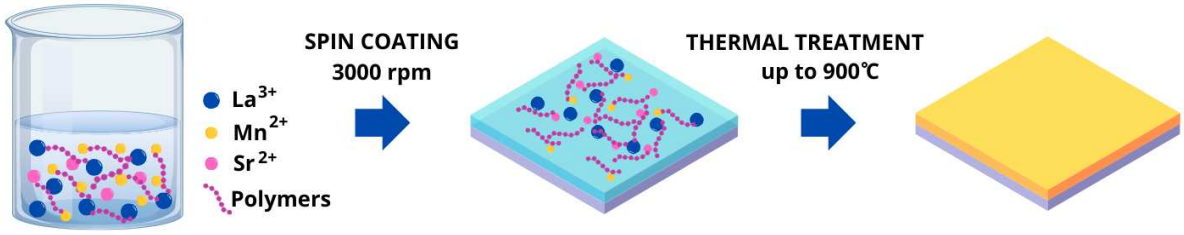

Figure 1. Schematic presentation of epitaxial film deposition process

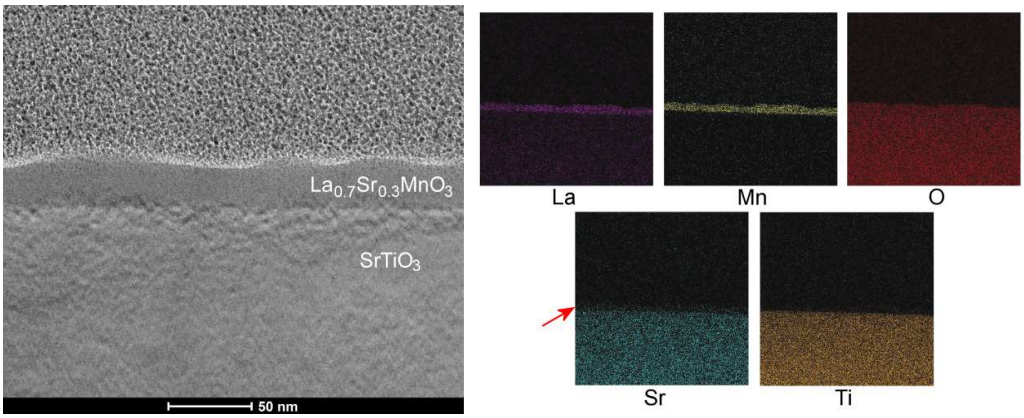

(a) (b)

Figure 2. Cross-sectional TEM micrograph of annealed $La_{0.7}Sr_{0.3}MnO_3$ film deposited on single crystal $SrTiO_3$ (001) substrate (a) with corresponding EDS elemental maps (b)

The magnetic properties of the manganite based thin films were measured using a MPMS3 commercial superconducting quantum interferometer device (SQUID) magnetometer (MPMS3, Quantum Design, San Diego, CA, USA). MPMS3 magnetometer enables measurements of magnetization in the temperature range of 1.8–400 K with the field applied parallel (in-plane) and perpendicular (out-of-plane) to the film surface. The angle dependence of the magnetic moment in the LSMO thin films at the room temperature was measured by a vibrating sample magnetometer (VSM, 8607, Lake Shore Cryotronics, Westerville, OH, USA). Resistivity as well as sheet resistance of the $La_{1-x}Sr_xMnO_3$ thin films was measured by the standard four-probe method on Ossila instrument.

III. Results and discussion

3.1. Structural characterization

The cross sections of the deposited $La_{1-x}Sr_xMnO_3$ (LSMO, where x = 0, 0.1, 0.3 and 0.5) thin films on the single crystal $SrTiO_3$ (001) substrate were examined by TEM. A typical TEM image of the $La_{0.7}Sr_{0.3}MnO_3$ thin film annealed at 900 °C is shown in Fig. 2a. It can be seen that the obtained film is homogeneously deposited on the substrate with a thickness of ~30 nm, having a well-defined interface and uniform and crack-free surfaces. EDS elemental maps corresponding to the area presented in the TEM micrograph (Fig. 2b) indicate a uniform distribution of elements over the film cross-section. Besides, some amounts of Sr can be seen in the film structure depicted by the red arrow in Fig. 2b.

XRD analyses were used to follow the structural changes of the deposited LSMO films on the single crystal $SrTiO_3$ (001) during annealing. The room temperature XRD patterns of the as-prepared LSMO thin films (heated at 750 °C for 1 h) confirm preferential c-axis film orientation along with the crystallographic [001] direction of the STO substrate. As an example, the XRD pattern of the $La_{0.7}Sr_{0.3}MnO_3$ film is shown in Fig. 3 - the logarithmic scale of the y-axis was used to better

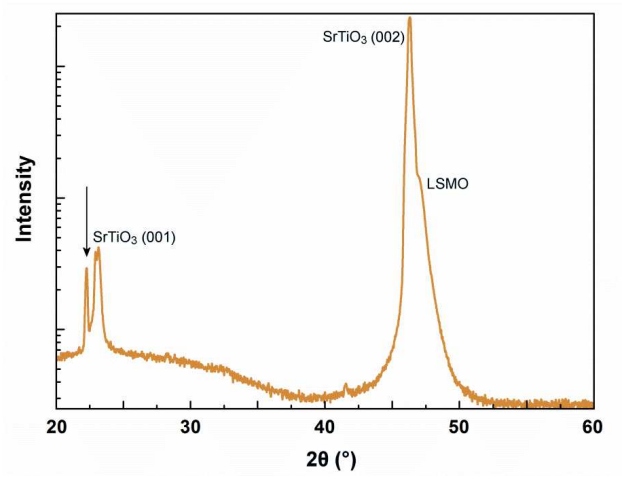

Figure 3. XRD pattern of as-prepared $La_{0.7}Sr_{0.3}MnO_3$ thin film on STO (001) substrate (y-axis has logarithmic scale and arrow indicates the presence of LMO non-stoichiometric phase)

observe the possible presence of XRD peaks of a secondary phase. The presence of small amount of non-stoichiometric LMO phase [15,22] can be associated with low-intensity XRD peak at ~22.5° (indicated with an arrow in Fig. 3). The appearance of this XRD peak could be related to incomplete film structure formation and the incorporation of a higher amount of different defects, causing a slight deviation from perfect epitaxial growth. This distorted perovskite structure consists of corner-sharing MnO_6 octahedra and La(Sr) cations occupying the 12-fold coordination site formed in the centre of eight such octahedra [23]. In theory, La-manganite can be considered as a structure derived from the elementary cubic cell with a lattice parameter of ~3.944 Å [24], where La^{3+} and Mn^{3+} are slightly displaced from their ideal positions, but the precise definition of phase is usually complicated. Thus, for the sake of simplicity, the structure of $La_{1-x}Sr_xMnO_3$ films on STO substrate is usually defined as pseudocubic.

For the obtained LSMO films, it is expected that the in-plane lattice constants a and b are well strained to

the STO substrate resulting in a change of lattice constant in the out-of-plane direction [25]. An increase in the out-of-plane lattice constant c characterizes the undoped LMO films, having larger lattice parameter of pseudocubic phase (~3.944 Å) than cubic STO substrate (3.905 Å) and a lattice mismatch of $\delta_{STO} = -1.0\%$. Substitution of La^{3+} (1.36 Å) with larger Sr^{2+} (1.44 Å) ions in LMO is accompanied by the conversion of manganese ions from Mn^{3+} to Mn^{4+} and contraction of the unit cell since the ionic radius of Mn^{4+} (0.53 Å) is much smaller than that of Mn^{3+} (0.65 Å) and the Jahn-Teller distortion of MnO_6 octahedra due to the presence of Mn^{4+} ions is less pronounced [26,27]. Thus, bulk $La_{0.7}Sr_{0.3}MnO_3$ has a rhombohedral perovskite structure that can be approximated as pseudocubic, with unit cell parameter $a = 3.873$ Å and $\alpha = 90.26°$ [28,29], and due to the corresponding lattice mismatch of $\delta_{STO} = +0.8\%$ the contraction of the unit cell in the out-of-plane direction (decrease of lattice constant c) is expected in LSMO film with a higher amount of Sr, deposited on the STO (001) substrate. The calculated out-of-plane lattice constant c of the as-prepared $La_{0.7}Sr_{0.3}MnO_3$ thin film (heated at 750 °C) is ~3.88 Å and corresponds to the lattice parameter of bulk $La_{0.7}Sr_{0.3}MnO_3$. However, the calculated lattice constant c of the as-prepared $La_{0.7}Sr_{0.3}MnO_3$ thin film is almost the same as that for the as-prepared pure $LaMnO_3$ thin film (heated at 750 °C) [14] even though it is mentioned that Sr-addition contracts the LMO lattice. Thus, the reason might be the formation of an imperfect crystal structure with some disoriented areas, non-stoichiometric LMO phases and defects created just to support the epitaxial growth of the as-prepared LSMO films.

The growth by vapour deposition techniques (PLD, MBE etc.), in which atoms from the gas phase are transported and deposited onto a substrate to form a thin film, is usually a high-energy process carried out under lower oxygen content in comparison to chemical solution deposition [27,30]. In the modified sol-gel method, so-called polymer assisted deposition, the polymers are used to form covalent complexes with metal cations and thus inactivate them. The coordination between the polymers and the metal ions prevents the nucleation of LMO-based films before the decomposition of the polymers and, in this way, controls the film deposition process. The used polymers are decomposed into volatile species, usually at temperatures up to 600 °C, and the released cations diffuse towards the substrate and incorporate into the film structure. The formation and crystallization of epitaxial LMO-based films are complicated and relatively slow processes [31,32]. Thus, the formation of an imperfect crystal structure at lower temperatures (up to 750 °C) can be expected, since different defects (such as point defects, planar defects, dislocations etc.) can be incorporated during this low-energy process [32–34]. This kind of structure is schematically shown in Supplementary material[§] (Fig. S1a), where disordered regions are marked with red rectangles. It was already mentioned [14,32,35] that epitaxial growth of LMO film on top of the STO (001) substrate could produce energetically unfavourable LMO cell compression in the ab plane, which causes the formation of a non-stoichiometric phase that allows relaxation of this stress through introduction of La^{3+} and/or O^{2-} vacancies and the transition of Mn^{3+} to Mn^{4+}.

Rearrangement of the obtained film structures, improved crystallinity and the achievement of high-quality epitaxial (or highly oriented) films can be expected only at higher temperatures [36]. In the first step, at intermediate temperatures (i.e. 800–850 °C), the non-stoichiometry of LMO film can be partially reduced (Supplementary material, Fig. S1b) by eliminating potential La^{3+} vacancies according to the following equation:

$$V_{La}''' + 2\,V_O^{\bullet\bullet} + 2\,Mn_{Mn}^{\bullet} + La_2O_3 \rightarrow \\ \rightarrow 2\,La_{La}^{\times} + 2\,Mn_{Mn}^{\times} + \frac{1}{2}\,O_2 \qquad (1)$$

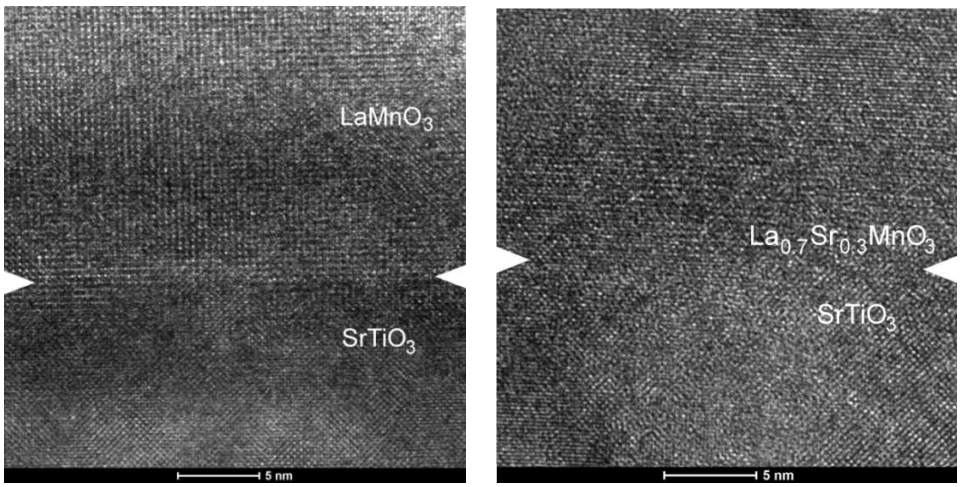

Figure 4. Cross-sectional HRTEM micrographs of LaMnO3 (left) and $La_{0.7}Sr_{0.3}MnO_3$ (right) thin films on STO (001) substrate annealed at 900 °C

Complete structural rearrangements are expected with further temperature increase (Supplementary material, Fig. S1c), which was confirmed by the movement of the characteristic XRD peak from ~46.8° in the as-prepared LMO film to ~45.8° in the LMO film annealed at 900 °C [14].

In accordance with the above mentioned, the as-prepared LSMO films were annealed in air at 800, 850 and 900 °C. The epitaxial nature of the deposited LSMO thin films was confirmed with HRTEM analysis. Figure 4 shows HRTEM micrographs of the thin $LaMnO_3$ and $La_{0.7}Sr_{0.3}MnO_3$ films deposited by PAD on the STO (001) substrates annealed at 900 °C. A highly oriented structure along the [001] direction with clean and well defined interfaces between the deposited film and substrate is noticeable.

XRD patterns (selected 2θ ranges) of the epitaxial $La_{0.7}Sr_{0.3}MnO_3$ films annealed at different temperatures are shown in Fig. 5. After annealing at 800 °C, the high orientation of the LSMO film is preserved, but the XRD peaks of the non-stoichiometric phase gradually disappear, the intensity of the XRD peak at ~46.8° (c = 3.88 Å) decreases and XRD peak at ~46.0° (c = 3.93 Å) appears indicating obvious structural rearrangements. Additional thermal treatment at 800 °C provided more energy to rearrange the structure and improve cation stoichiometry [14]. It seems that this structure has a lower amount of defects and is close to the orthorhombic (*Pbnm*) LMO phase that was also proposed for some epitaxial $LaMnO_3$ films annealed at lower temperatures [34]. In addition, it is interesting that similar changes were observed for the undoped LMO film after annealing at 800 °C [14] and could indicate that the rearrangements at this stage are not influenced dominantly by Sr-doping. This is unexpected since it is well known that substitution of La^{3+} with Sr^{2+} causes the transition of Mn^{3+} to Mn^{4+}, changing the Jahn-Teller distortion and decreasing lattice volume [24].

The observed increase of the lattice parameter after annealing at 800 and 850 °C can be explained by the slow reduction of the non-stoichiometry through the elimination of potential La^{3+} vacancies according to Eq. 1, but also by the limited formation of Mn^{4+} ions (which is expected in Sr-doped LMO structures). This is due to the fact that Sr-doping in this stage favours the formation of defect structures with O^{2-} vacancies (Eq. 2) instead of the simple conversion of Mn^{3+} to Mn^{4+} ions (Eq. 3):

$$2\,La_{La}^{\times} + O_O^{\times} + 2\,SrO \rightarrow 2\,Sr_{La}' + V_O^{\bullet\bullet} + La_2O_3 \quad (2)$$

$$2\,La_{La}^{\times} + 2\,Mn_{Mn}^{\times} + \frac{1}{2}\,O_2 + 2\,SrO \rightarrow 2\,Sr_{La}' + 2\,Mn_{Mn}^{\bullet} + La_2O_3 \quad (3)$$

Thus, at higher temperatures, the structure is rearranged slowly, at first decreasing the non-stoichiometry without increasing Mn^{4+} content (schematically presented in the Supplementary material, Figs. S2a and S2b). These changes are correlated with the movement of the characteristic XRD peak from ~46.8° in the as-prepared LSMO film to ~45.8° in the annealed LSMO film at 850 °C. The expected decrease of the lattice parameter (i.e. movement of XRD peak to higher angles) was observed after annealing at 900 °C (Fig. 5). The reason is the elimination of O^{2-} vacancies and the conversion of Mn^{3+} to Mn^{4+} according to the following equation:

$$2\,Mn_{Mn}^{\times} + V_O^{\bullet\bullet} \rightarrow 2\,Mn_{Mn}^{\bullet} \quad (4)$$

These changes are schematically shown in the Supplementary material, Fig. S2c.

Since the observed structural changes during annealing at temperatures from 750 to 900 °C should have influence on electric properties, the electrical resistivity (sheet resistance) of the prepared films was measured (Fig. 6). It is obvious that the resistivity decreases with the increase of annealing temperature which is an indication of structural rearrangement. Very steep decrease can be seen for the $La_{0.5}Sr_{0.5}MnO_3$ film (Fig. 6), which also has the lower crystallinity at 750 °C in comparison to other Sr-doped films. Thus, it can be concluded that the as-deposited films with higher Sr content have

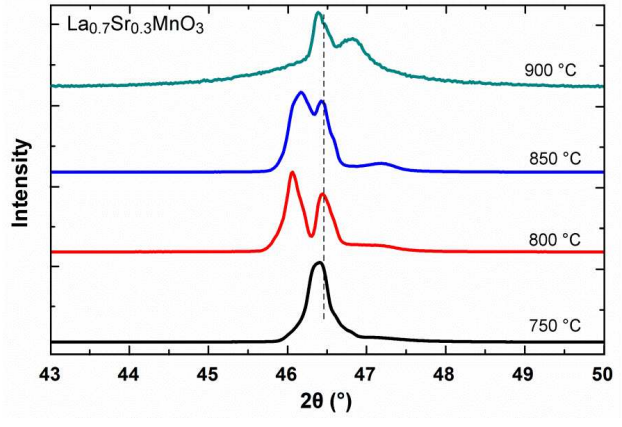

Figure 5. XRD patterns (selected areas) of as-prepared and annealed $La_{0.7}Sr_{0.3}MnO_3$ thin films on the STO (001) substrate (dashed line indicates the substrate peak)

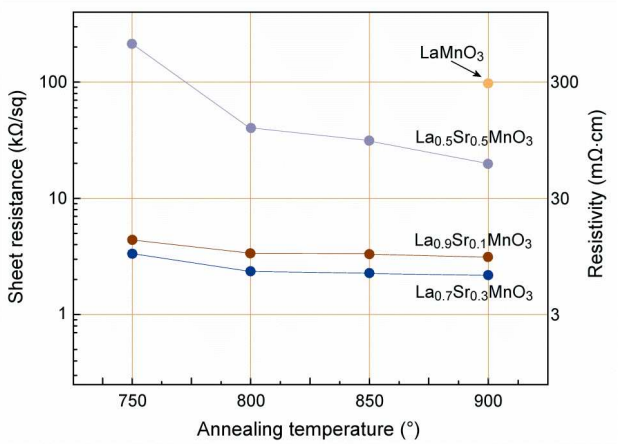

Figure 6. Electrical resistivities of of LSMO thin films annealed at different temperatures

more disordered structure. The $LaMnO_3$ film annealed at 900 °C has the highest resistivity and, as expected, resistivity decreases with Sr addition for lower Sr-content (the $La_{0.9}Sr_{0.1}MnO_3$ and $La_{0.7}Sr_{0.3}MnO_3$ films) due to the hopping induced by higher amount of Mn^{4+} ions. The resistivities of the samples are similar to the values for the corresponding epitaxial thin films obtained by vapour deposition techniques [37,38].

It is important to underline that with the increase in Sr content, bulk $La_{1-x}Sr_xMnO_3$ undergoes an orthorhombic-to-rhombohedral phase transition for $x > 0.17$ and the appearance of the rhombohedral ($R\bar{3}c$) LMO phase can be expected in the bulk $La_{0.7}Sr_{0.3}MnO_3$ sample [39,40]. The presence of orthorhombic and coexistence of orthorhombic and rhombohedral phases was also reported for Sr-doped LMO films [34,39].

The effect of Sr-doping is clearly visible only for the samples annealed at 850 and 900 °C (Figs. 7 and 8). XRD patterns (selected 2θ ranges) of the thin $La_{0.7}Sr_{0.3}MnO_3$ and $La_{0.5}Sr_{0.5}MnO_3$ films annealed at 850 °C (Fig. 7) reveal the increased intensity of the XRD peak at ~47° which could be an indication of an orthorhombic-to-rhombohedral phase transition. In addition, there are obvious differences in XRD patterns of the LSMO films with different Sr content. The position of the characteristic XRD peak of LMO phase is at ~46.1° (c = 3.93 Å) for the $LaMnO_3$ and $La_{0.9}Sr_{0.1}MnO_3$ samples and shifts to ~47.1° (c = 3.87 Å) for the $La_{0.7}Sr_{0.3}MnO_3$ and $La_{0.5}Sr_{0.5}MnO_3$ films (Fig. 8). The obtained values are very close to the pseudocubic lattice parameters of bulk $LaMnO_3$ and $La_{0.7}Sr_{0.3}MnO_3$, respectively [29,41]. However, those characteristic peaks are accompanied by a small secondary XRD peak (on the opposite side with respect to the STO substrate peak - see red arrows in Fig. 8). This second peak is clearly visible in all XRD patterns of the LSMO films annealed at 900 °C, which indicates the possible coexistence of orthorhombic and rhombohedral phases. Indeed, the orthorhombic phase seems to be the dominant one in the thin $LaMnO_3$ and $La_{0.9}Sr_{0.1}MnO_3$ films, but the rhombohedral phase is more pronounced in the samples with higher Sr-content. These films are constrained in *ab* plane (in-plane) due to the high lattice constant of the cubic STO substrate forcing the structural accommodation in the out-of-plane direction. This led to a decrease in lattice parameter c and a decrease in LSMO lattice volume, which could explain the formation of the phases with lower symmetry.

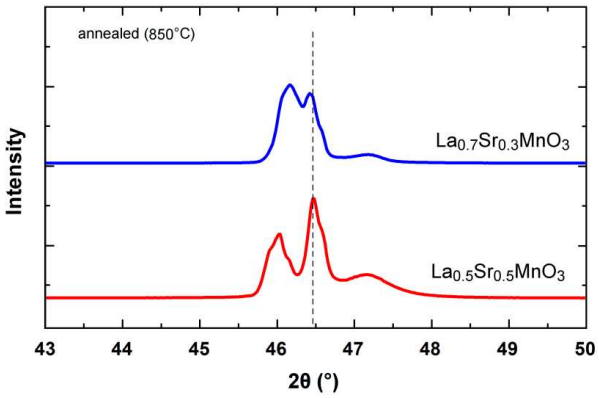

Figure 7. XRD patterns of $La_{0.7}Sr_{0.3}MnO_3$ and $La_{0.5}Sr_{0.5}MnO_3$ thin films annealed at 850 °C (dashed line indicates the substrate)

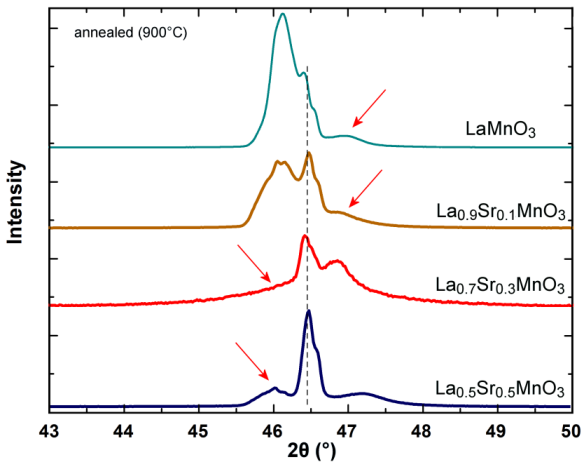

Figure 8. XRD patterns of LSMO thin films annealed at 900 °C (dashed line indicates the substrate)

3.2. *Magnetic properties*

Figure 9a shows the measured hysteresis loops of $M(H)$ at 5, 100 and 250 K of the epitaxial $La_{0.9}Sr_{0.1}MnO_3$ film deposited on the STO (001) substrate, which look typical for LSMO system with such Sr concentration. Well-defined hysteresis loops showing ferromagnetic behaviour are observed at the lower temperatures (5 and 100 K). Increasing the temperature up to 250 K causes a considerable decrease in magnetization and coercivity, due to approaching the paramagnetic state transition. This is in agreement with the literature data for bulk lanthanum manganite, since bulk $La_{0.9}Sr_{0.1}MnO_3$ is paramagnetic at room temperature [42]. Indeed, the temperature dependence of magnetic moment $M(T)$ points to the magnetic ordering temperature of 265 ± 4 K. However, if compared to other results (for example in Asamitsu *et al.* [43] as representative for bulk samples), $La_{0.9}Sr_{0.1}MnO_3$ should have somewhat lower magnetic transition temperature and the saturation magnetization than measured here. This comparison suggests that here the stoichiometry might be slightly different from the nominal ideal one, or that some additional oxygen defects due to the surface geometry could easily change the magnetic interactions. Zero field cooled (ZFC) and field cooled (FC) curves measured in three different magnetic fields are shown in Fig. 9b. For lower fields the ZFC-FC splitting is characteristic for ferromagnet, while there is no irreversibility in the full temperature interval for field of 1 kOe. Despite the coercive field of 300 Oe, the reversibility appears for field less than 1 kOe, due to the steep rise on hysteresis loops at small fields.

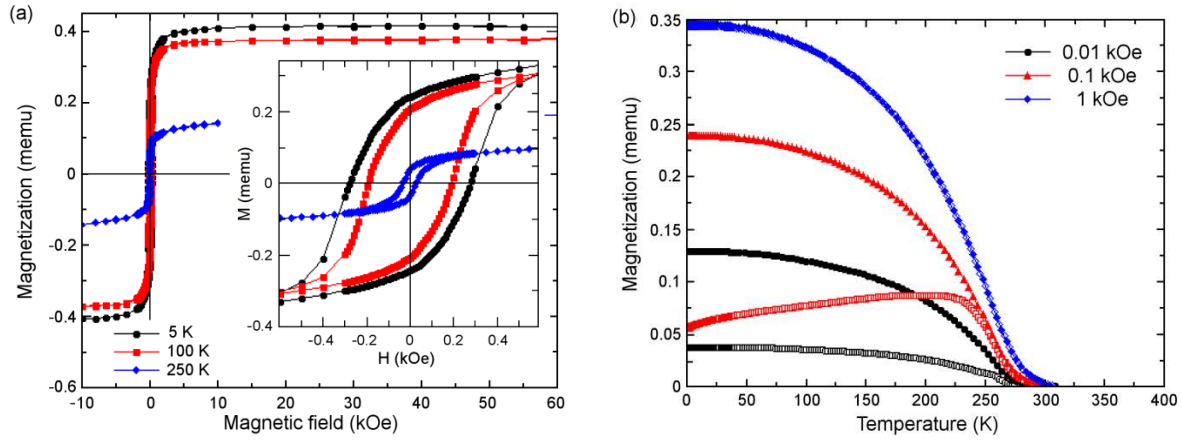

Figure 9. Hysteresis curves measured at 5, 100 and 250 K with inset showing zoomed range around low external fields (a) and temperature-dependent ZFC and FC magnetizations in field of 0.01, 0.1 and 1 kOe (b) for epitaxial $La_{0.9}Sr_{0.1}MnO_3$ film annealed at 900 °C

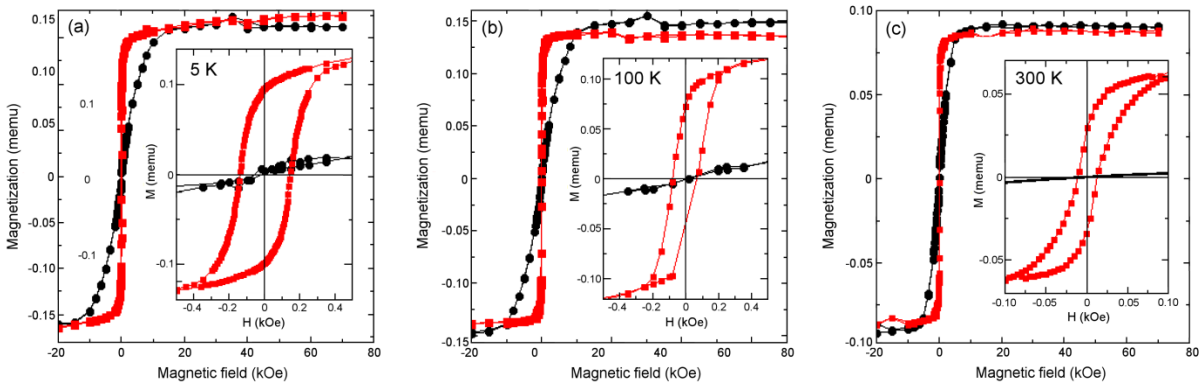

Figure 10. Hysteresis loops measured in-plane (red symbols) and out-of-plane (black symbols) at: 5 K (a), 100 K (b) and 300 K (c) for epitaxial $La_{0.7}Sr_{0.3}MnO_3$ film annealed at 900 °C

The epitaxial $La_{0.7}Sr_{0.3}MnO_3$ thin film explored more thoroughly, since it is ferromagnetic at ambient conditions and thus appropriate for possible applications. The first of all, measured hysteresis loops of the epitaxial $La_{0.7}Sr_{0.3}MnO_3$ film at 5, 100 and 300 K when the magnetic field was applied parallel (in-plane) and perpendicular (out-of-plane) to the film surface are shown in Fig. 10. It is obvious that the $La_{0.7}Sr_{0.3}MnO_3$ thin film is ferromagnetic at room temperature. Assuming that the thicknesses of the films $La_{0.9}Sr_{0.1}MnO_3$ and $La_{0.7}Sr_{0.3}MnO_3$ are approximately similar as well as the surface areas, we can see that $La_{0.7}Sr_{0.3}MnO_3$ has somewhat smaller saturation magnetization. But, this is opposite to the already known behaviour of bulk LSMO system, where higher amount of Sr should increase the magnetization, which therefore demands further explanation. The observation tells that $La_{0.9}Sr_{0.1}MnO_3$ film has actually larger volume than $La_{0.7}Sr_{0.3}MnO_3$. Nevertheless, for the $La_{0.7}Sr_{0.3}MnO_3$ the measured magnetic moment divided by volume and density of the film gives the mass magnetization in saturated state of 85±7 emu/g that fits perfectly within the saturation magnetization values of bulk compound produced with different synthesis methods (75–100 emu/g). The produced films have magnetic properties in agreement with the known phase diagram and the literature data [9,42,44], and from the observed magnetic transition temperatures, 265 ± 4 K and 360 ± 4 K for the $La_{0.9}Sr_{0.1}MnO_3$ and $La_{0.7}Sr_{0.3}MnO_3$ films, respectively, it is confirmed that the amount of Sr incorporated during preparation is very near to the desired one, and that $La_{0.7}Sr_{0.3}MnO_3$ is tuned to the maximal magnetic transition temperature within LSMO system.

LSMO members are usually very soft ferromagnets in bulk form, so that the increased coercive field of 140 Oe shows that thin film geometry contributes to the difficulty of the magnetization reversal through formation of magnetic hard axis. Indeed, measurements of magnetization in direction parallel and perpendicular to the thin film surface, as shown in Fig. 10, suggest the presence of an easy plane magnetization and a hard axis perpendicular to the thin film. The difference of magnetization between two directions is very pronounced as it can be seen in insets of each panel (Fig. 10) through small slope without open hysteresis (black curves) for out-of-plane direction in strong contrast to the in-plane steep hysteresis curves. Such large anisotropy can be explained only with considerable magnetocrystalline anisotropy that favours in-plane magnetization. It was already confirmed that anisotropic

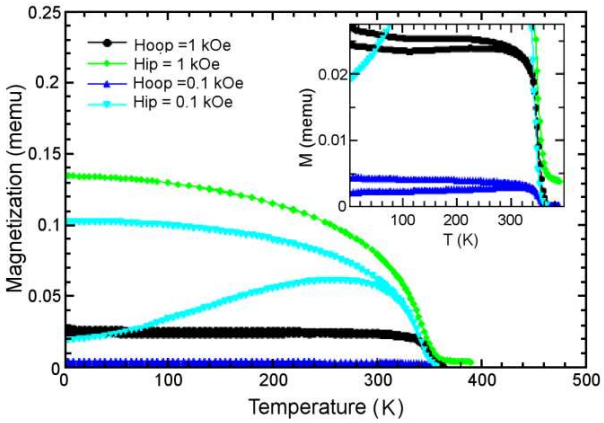

Figure 11. Temperature-dependent ZFC and FC magnetizations with external field of 0.1 and 1 kOe measured in-plane and out-of-plane directions for $La_{0.7}Sr_{0.3}MnO_3$ film annealed at 900 °C

magnetization can be induced by strain [45], which is here achieved with matching the lattice of the film with the substrate lattice beneath. It should be noted that demagnetization factor is far below the value which would produce such large observed anisotropy and also it is well below the influence of intrinsic magnetocrystalline anisotropy of the bulk LSMO, which leads to conclusion that the measured anisotropy comes mainly from the magnetocrystalline anisotropy of the thin film LSMO.

The field cooled (FC) and zero field cooled (ZFC) magnetizations as a function of the temperature from 5 to 400 K under applied in-plane and out-of-plane magnetic fields of 0.1 and 1 kOe are shown in Fig. 11. The observed sharp rise in magnetization due to the paramagnetic to ferromagnetic transition with cooling corresponds to the Curie temperature (T_C) of ~360 K. For the in-plane magnetic field of 1 kOe, both ZFC and FC magnetization curves coincide well with each other, but a bifurcation between them is clearly observed for the field of 0.1 kOe (typical behaviour for doped lanthanum manganites [46]). However, inset of Fig. 11 shows much lower magnetization in the out-of-plane direction, only 5% of the in-plane in small fields, with the well observable ZFC-FC splitting in broad temperature range from 2 up to 300 K. This confirms again the presence of the magnetocrystalline anisotropy in the prepared epitaxial $La_{0.7}Sr_{0.3}MnO_3$ thin film. With increasing field, the in-plane and out-of-plane ZFC-FC curves become closer, and they would become the same at 15 kOe as it is visible on hysteresis loops, which points to the considerable anisotropy field induced by strain in natively soft ferromagnet.

More detailed insight into magnetic anisotropy is obtained with measuring the angle dependence of the magnetic moment, shown in Fig. 12. These measurements were performed at room temperature and the background magnetic moment of the substrate was not removed. Nevertheless, this is reliable for the qualitative discussions, especially because of the considerable prevailing of the ferromagnetic moment of thin film at such relatively small magnetic fields. Angle is defined as the one between the magnetic field and the normal on the thin film plane, where the magnetic moment is measured in the direction of applied magnetic field. The presented results indicate a strong influence of the rotation of the sample on the measured magnetic moment (Fig. 12a). The shape of the curve uniquely confirms the preferential orientation of magnetization in plane of the prepared $La_{0.7}Sr_{0.3}MnO_3$ film, with a clear indication of a single hard axis perpendicular to the film. Additionally, the hysteresis loops at room temperature obtained by VSM presented in Fig. 12b also show an obvious difference of the in-plane and out-plane magnetization, showing anisotropic hysteresis loops. Moreover, the application of the field using classical electromagnet allows the measurement of open hysteresis loops without superconducting magnet artefacts, enabling thus the clear and precise observation of hysteresis at the room temperature. These properties are favourable for application in spintronic devices. Moreover, the difference between in-plane and out-of-plane magnetizations related to anisotropy in LSMO film structure is essential for achieving high-density, high-stability and low-power-consumption spintronic devices [47].

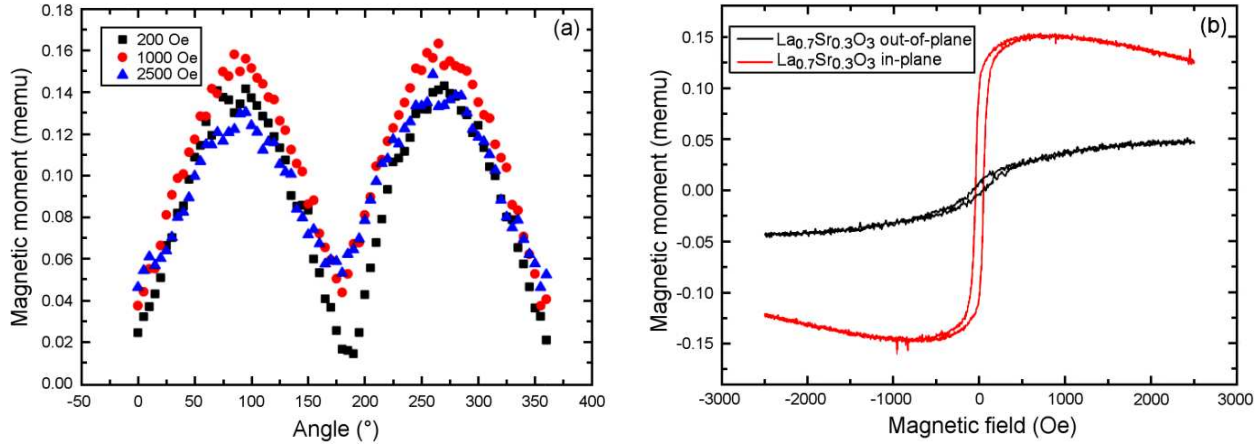

Figure 12. Angle dependence of magnetic moment (a) and VSM hysteresis loops at 300 K obtained with in-plane and out-of-plane magnetic fields of epitaxial $La_{0.7}Sr_{0.3}MnO_3$ film annealed at 900 °C

IV. Conclusions

In this paper, epitaxial $La_{1-x}Sr_xMnO_3$ (LSMO, where x = 0, 0.1, 0.3 and 0.5) thin films were successfully prepared by modified sol-gel method, so-called polymer assisted deposition (PAD) method on the single crystal $SrTiO_3$ (001) substrate. The XRD patterns of the as-prepared LSMO thin films (heated at 750 °C for 1 h) confirm preferential c-axis film orientation along with the crystallographic [001] direction of the STO substrate. However, the as-prepared LSMO films are characterized by the formation of an imperfect crystal structure with some disoriented areas, an impurity phase and defects created just to support the epitaxial growth. The prepared thin films were multiple annealed at different temperatures up to 900 °C, in order to investigate structural changes during post-annealing treatment. At lower annealing temperature (800 °C) the observed rearrangements (elimination of defects and formation of unit cell closer to the stoichiometric phase) were not influenced dominantly by Sr-doping. The possible coexistence of orthorhombic and rhombohedral lanthanum manganite phases was noticed at higher annealing temperatures. Thus, the orthorhombic phase seems to be the dominant one in the epitaxial $LaMnO_3$ and $La_{0.9}Sr_{0.1}MnO_3$ films, but the rhombohedral phase is more pronounced in the samples with higher Sr-content.

Well defined hysteresis loops with typical ferromagnetic behaviour were observed at the lower temperatures (5 K and 100 K) for the epitaxial $La_{0.9}Sr_{0.1}MnO_3$ film and transition to paramagnetic state was observed below room temperature, i.e. 265 ± 4 K. On the other hand, the $La_{0.7}Sr_{0.3}MnO_3$ thin film is ferromagnetic at room temperature (with the transition temperature 360 ± 4 K). Measurements of magnetization in direction parallel (in-plane) and perpendicular (out-of-plane) to the thin film surface suggest the presence of an easy plane magnetization and a hard axis perpendicular to the thin film. Such large anisotropy can be explained only with considerable magnetocrystalline anisotropy that favours in-plane magnetization.

Acknowledgement: This research was supported by the Science Fund of the Republic of Serbia, PRIZMA PROMTEH, #GRANT No 7383, "Processing of manganite thin film heterostructures and control of their physical properties by light stimuli". We also acknowledge the financial support provided by the Serbian Academy for Science and Arts, Project F-137, as well as COST Project CA23136 (CHIROMAG). P. Šenjug and D. Pajić acknowledge the support of project CeNIKS, cofinanced by the Croatian Government and the European Union through the European Regional Development Fund - Competitiveness and Cohesion Operational Programme (Grant KK.01.1.1.02.0013).

§ Supplementary data can be downloaded using following link: https://t.ly/plFoQ

References

1. W. Norfazilah, W. Ismail, "Sol-gel technology for innovative fabric finishing - A review", *J. Sol-Gel Sci. Technol.*, **78** (2016) 698–707.
2. T. Schneller, R. Waser, M. Kosec, D. Payne, *Chemical solution deposition of functional oxide thin films*, Springer, Vienna, 2016.
3. I. Bretos, R. Jiménez, J. Ricote, A.Y. Rivas, M. Echániz-Cintora, R. Sirera, M. Lourdes Calzada, "Low-temperature sol-gel methods for the integration of crystalline metal oxide thin films in flexible electronics", *J. Sol-Gel Sci. Technol.*, **107** (2023) 269–277.
4. W. Eerenstein, M. Wiora, J.L. Prieto, J.F. Scott, N.D. Mathur, "Giant sharp and persistent converse magnetoelectric effects in multiferroic epitaxial heterostructures", *Nat. Mater.*, **6** (2007) 348.
5. J. Ma, J. Hu, Z. Li C.-W. Nan, "Recet progress in multiferroic magnetoelectric composites: From bulk to thin films", *Adv. Mater.*, **23** (2011) 1062–1087.
6. C. Zhang, S. Ding, K. Qiao, J. Li, Z. Li, Z. Yin, J. Sun, J. Wang, T. Zhao, F. Hu, B. Shen, "Large low-field magnetoresistance (LFMR) effect in free-standing $La_{0.7}Sr_{0.3}MnO_3$ films", *ACS Appl. Mater. Interfaces*, **13** [24] (2021) 28442–28450.
7. P. Hou, Y. Liu, Z. Liu, C. Zhu, Y. Li, Z. Xi, Y. Han, J. Li, M.-R. Li, J. Zhou, L. Chen, Y. Deng, Y. Yang, J.-M. Liu, D. Wu, "Ferromagnetism with strong perpendicular magnetic anisotropy in epitaxial $SrMn_{0.3}Ir_{0.7}O_3$ perovskite films pengxiang", *Phys. Rev. Appl.*, **18** (2022) 054083.
8. L.G. Enger, S. Flament, I.-N. Bhatti, B. Guillet, M.L.C. Sing, V. Pierron, S. Lebargy, J.M. Diez, A. Vera, I. Martinez, R. Guerrero, L. Perez, P. Perna, J. Camarero, R. Miranda, M.T. Gonzalez, L. Mechin, "Sub-nT resolution of single layer sensor based on the AMR effect in $La_{2/3}Sr_{1/3}MnO_3$ thin films", *IEEE Trans. Magn.*, **58** [2] (2022) 4001204.
9. S.K. Chaluvadi, Z. Wang, L.M. Carvalho de Araújo, P. Orgiani, V. Polewczyk, G. Vinai, O. Rousseau, V. Pierron, A. Pautrat, B. Domenges, D.G. Schlom, L. Mechin, "Integration of epitaxial $La_{2/3}Sr_{1/3}MnO_3$ thin films on silicon-on-sapphire substrate for MEMS applications", *Appl. Surface Sci.*, **579** (2022) 152095.
10. C. Aruta, M. Angeloni, G. Balestrino, N.G. Boggio, P.G. Medaglia, A. Tebano, "Preparation and characterization of $LaMnO_3$ thin films grown by pulsed laser deposition", *J. Appl. Phys.*, **100** (2006) 023910.
11. M.H. Aguirre, S. Canulescu, R. Robert, N. Homazava, D. Logvinovich, L. Bocher, Th. Lippert, M. Döbeli, A. Weidenkaff, "Structure, microstructure, and high-temperature transport properties of $La_{1-x}Ca_xMnO_{3-\delta}$ thin films and polycrystalline bulk materials", *J. Appl. Phys.*, **103** (2008) 013703.
12. A. Gupta, T.R. McGuire, P.R. Duncombe, M. Rupp, J.Z. Sun, W.J. Gallagher, G. Xiao, "Growth and giant magnetoresistance properties of La-deficient $La_xMnO_{3-\delta}$ ($0.67 \leq x \leq 1$) films", *Appl. Phys. Lett.*, **67** (1995) 3494–3496.
13. T.F. Zhou, G. Li, X.G. Li, "Self-generated in-plane superlattice in relaxed epitaxial $La_{0.67}Sr_{0.33}MnO_3$ films", *Appl. Phys. Lett.*, **90** (2007) 042512.
14. J. Vukmirović, S. Joksović, D. Piper, A. Nesterović, M.

Novaković, S. Rakić, M. Milanović, V.V. Srdić, "Epitaxial growth of $LaMnO_3$ thin films on different single crystal substrates by polymer assisted deposition", *Ceram. Int*., **49** (2023) 2366–2372.
15. A. Boukhachem, A. Ziouche, M. Ben Amor, O. Kamoun, M. Zergoug, H. Maghraoui-Meherzi, A. Yumak, K. Boubaker, M. Amlouk, "Physical investigations on perovskite $LaMnO_{3-\delta}$ sprayed thin films for spintronic applications", *Mater. Res. Bull*., **74** (2016) 202–211.
16. Y. Tokura, Y. Tomioka, "Colossal magnetoresistive manganites", *J. Magn. Magn. Mater*., **200** (1999) 1–23.
17. Y. Tokura, N. Nagaosa, "Orbital physics in transition-metal oxides, *Science*, **288** (2000) 462–468.
18. E. Dagotto, T. Hotta, A. Moreo, "Colossal magnetoresistant materials: The key role of phase separation", *Phys. Reports*, **344** (2001) 1–153.
19. D. Rasic, R. Sachan, N.K. Temizer, "Oxygen effect on the properties of epitaxial (110) $La_{0.7}Sr_{0.3}MnO_3$ by defect engineering", *ACS Appl. Mater. Interfaces*, **10** [24] (2018) 21001–21008.
20. R. Trappen, A.C. Garcia-Castro, V.T. Tra, C.-Y. Huang, W. Ibarra-Hernandez, J. Fitch, S. Singh, J. Zhou, G. Cabrera, Y.-H. Chu, J.M. LeBeau, A.H. Romero, M.B. Holcomb, "Electrostatic potential and valence modulation in $La_{0.7}Sr_{0.3}MnO_3$ thin films", *Sci. Reports*, **8** (2018) 14313.
21. J. Zang, J.C. Ma, "Manipulating the magnetic and electric transport properties of $La_{0.7}Sr_{0.3}MnO_3$ epitaxial thin film through ionic liquid-gated technology", *Thin Solid Films*, **768** (2023) 139699.
22. F. Abbattista, M. Lucco Borlera, "Reduction of $LaMnO_3$ - Structural features of phases $La_8Mn_8O_{23}$ and $La_4Mn_4O_{11}$", *Ceram. Int*., **7** [4] (1981) 137–141.
23. T. Chatterji, F. Fauth, B. Ouladdiaf, P. Mandal, B. Ghosh, "Volume collapse in $LaMnO_3$ caused by an orbital order-disorder transition", *Phys. Rev. B*, **68** (2003) 052406.
24. S.K. Chaluvadi, V. Polewczyk, A.Yu Petrov, G. Vinai, L. Braglia, J.M. Diez, V. Pierron, P. Perna, L. Mechin, P. Torelli, P. Orgiani, "Electronic properties of fully strained $La_{1-x}Sr_xMnO_3$ thin films grown by molecular beam epitaxy ($0.15 \leq x \leq 0.45$) ", *ACS Omega*, **7** (2022) 14571–14578.
25. W.S. Choi, D.W. Jeong, S.Y. Jang, Z. Marton, S.S.A. Seo, H.N. Lee, Y.S. Lee, "$LaMnO_3$ thin films grown by using pulsed laser deposition and their simple recovery to a stoichiometric phase by annealing", *J. Korean Phys. Soc*., **58** [3] (2011) 569–574.
26. S. Hebert, B. Wang, A. Maignan, C. Martin, R. Retoux, B. Raveau, "Vacancies at Mn-site in Mn^{3+} rich manganites: A route to ferromagnetism but not to metallicity", *Solid State Commun*., **123** (2002) 311–315.
27. Q. Sun, X. Luo, Q. Xia, Y. Guo, J. Su, Q. Li, G. Miao, "Enhanced ferromagnetism and conductivity in epitaxial $LaMnO_3$ thin films by oxygen-atmosphere annealing", *J. Magn. Magn. Mater*., **499** (2020) 166317.
28. S.W. Jin, G.Y. Gao, Z. Huang, Z.Z. Yin, X. Zheng, W. Wu, "Shear-strain-induced low symmetry phase and domain ordering in epitaxial $La_{0.7}Sr_{0.3}MnO_3$ thin films", *Appl. Phys. Lett*., **92** (2008) 261901.
29. S. Kumari, N. Mottaghi, C.-Y. Huang, R. Trappen, G. Bhandari, S. Yousefi, G. Cabrera, M.S. Seehra, M.B. Holcomb, "Effects of oxygen modification on the structural and magnetic properties of highly epitaxial $La_{0.7}Sr_{0.3}MnO_3$ (LSMO) thin films", *Sci. Reports*, **11** (2020) 3659.
30. T. Petrisor Jr., M.S. Gabor, A. Boulle, C. Bellouard, C. Tiusan, O. Pana, T. Petrisor, "Oxygen incorporation effects in annealed epitaxial $La_{(1-x)}Sr_xMnO_3$ thin films", *J. Appl. Phys*., **109** (2011) 123913.
31. A.K. Burrell, T.M. McClesky, Q.X. Jia, "Polymer assisted deposition, *Chem. Commun*., **11** (2008) 1271–1277.
32. J.M. Vila-Fungueirino, B. Rivas-Murias, J. Rubio-Zuazo, A. Carretero-Genevrier, M. Lazzari, F. Rivardulla, "Polymer assisted deposition of epitaxial oxide thin films", *J. Matter. Chem. C*, **6** (2018) 3834–3844.
33. J.M. Vila-Fungueirino, B. Rivas-Murias, B. Rodríguez-Gonzalez, O. Txoperena, D. Ciudad, L.E. Hueso, M. Lazzari, F. Rivadulla, "Room-temperature ferromagnetism in thin films of $LaMnO_3$ deposited by a chemical method over large areas", *ACS Appl. Mater. Interfaces*, **7** (2015) 5410–5414.
34. R. Rodriguez-Lamas, C. Pirovano, A. Stangl, D. Pla, R. Jonsson, L. Rapenne, E. Sarigiannidou, N. Nuns, H. Roussel, O. Chaix-Pluchery, M. Boudard, C. Jimenez, R.-N. Vannier, M. Burriel, "Epitaxial $LaMnO_3$ films with remarkably fast oxygen transport properties at low temperature", *J. Mater. Chem*., **9** (2021) 12721–12733.
35. D. Piper, J. Vukmirovic, I. Tokovic, A. Kukovecz, I. Szenti, M. Novakovic, M. Milanovic, V.V. Srdic, "Epitaxial bilayer $La_{0.7}Sr_{0.3}MnO_3/Ba_{0.7}Sr_{0.3}TiO_3$ thin films obtained by polymer assisted deposited", *Process. Appl. Ceram*., **17** [2] (2023) 197–202.
36. T.M. McCleskey, P. Shi, E. Bauer, M.J. Highland, J.A. Eastman, Z.X. Bi, P.H. Fuoss, P.M. Baldo, W. Ren, B.L. Scott, A.K. Burrell, Q.X. Jia, "Nucleation and growth of epitaxial metal-oxide films based on polymer-assisted deposition", *Chem. Soc. Rev.,* **43** (2014) 2141–2146.
37. P.R. Broussard, S.B. Qadri, V.M. Browning, V.C. Cestone, "Characterization of transport and magnetic properties in thin film $La_{0.67}(Ca_xSr_{1-x})_{0.33}MnO_3$ mixtures", *J. Appl. Phys.,* **85** (1999) 6563–6566.
38. T. Tsuchiya, T. Nakajima, K. Daoudi, T. Kumagai, "Electrical properties of the epitaxial $La_{1-x-y}Sr_xMnO_3$ films grown by excimer laser-assisted metal organic deposition", *Mater. Sci. Eng. B*, **144** (2007) 89–92.
39. J. Kreisel, G. Lucazeau, C. Dubourdieu, M. Rosina, F. Weiss, "Raman scattering study of $La_{0.7}Sr_{0.3}MnO_3/SrTiO_3$ multilayers", *J. Phys. Condens. Matter,* **14** (2002) 5201.
40. K. Guo, Y. Tao, Y. Liu, Y. Lyu, Z. Pan, "One-stage hydrothermal growth and characterization of epitaxial $LaMnO_3$ films on $SrTiO_3$ substrate", *Materials*, **15** (2022) 5928.
41. W.S. Choi, Z. Marton, S.Y. Jang, S.J. Moon, B.C. Jeon, J.H. Shin, S.S.A. Seo, T. W. Noh, K. Myung-Whun, H.N. Lee, "Effects of oxygen-reducing atmosphere annealing on $LaMnO_3$ epitaxial thin films", *J. Phys. D Appl. Phys*., **42** (2009) 165401.
42. J. Hemberger, A. Krimmel, T. Kurz, H.-A. Krug von Nidda, V. Yu. Ivanov, A.A. Mukhin, A.M. Balbashov, A. Loidl, "Structural, magnetic, and electrical properties of single-crystalline $La_{1-x}Sr_xMnO_3$ $0.4 < x < 0.85$", *Phys. Rev. B*, **66** (2002) 094410.
43. A. Asamitsu, Y. Moritomo, R. Kumai, Y. Tomioka, Y. Tokura, "Magnetostructural phase transitions in $La_{1-x}Sr_xMnO_3$ with controlled carrier density", *Phys. Rev. B*, **54** (1996) 1716–1723.
44. J.M.D. Coey, *Magnetism and Magnetic Materials*, Cam-

bridge University Press, Cambridge, UK, 2010.
45. H.S. Wang, Q. Li, K. Liu, C.L. Chien, "Low-field magnetoresistance anisotropy in ultrathin $Pr_{0.67}Sr_{0.33}MnO_3$ films grown on different substrates", *Appl. Phys. Lett*., **74** (1999) 2212–2214.
46. M. Muroi, R. Street, "Evolution of ferromagnetism in $LaMnO_{3+\delta}$", *Aust. J. Phys*., **52** (1999) 205–225.
47. S. Emori, U. Bauer, S.M. Ahn, E. Martinez, G.S.D. Beach, "Current-driven dynamics of chiral ferromagnetic domain walls", *Nat. Mater*., **12** (2013) 611–616.